Supporting Information

Multivalent ion-induced re-entrant transition of carboxylated cellulose nanofibrils and its influence on nanomaterials properties

Luis Valencia[a‡±], Emma M. Nomena[b,c‡], Susanna Monti[d‡],Walter Rosas-Arbelaez[e], Aji P. Mathew[a], Sugam Kumar[a,f‡]and Krassimir P. Velikov[b,c,g*]*

[a] Division of Materials and Environmental Chemistry, Stockholm University, Frescativägen 8,10691, Stockholm, Sweden Address here.
[b] Materials Technology and Chemistry, Alfa Laval Tumba AB, SE-14782 Tumba, Sweden
[c] Unilever Innovation Centre Wageningen, Bronland 14, 6708 WH Wageningen, the Netherlands
[d] Institute of Physics, University of Amsterdam, Science Park 904, 1098 XH Amsterdam, the Netherlands
[e] CNR-ICCOM – Institute of Chemistry of Organometallic Compounds, via Moruzzi 1, 56124 Pisa, Italy
[f] Department of Chemistry and Chemical Engineering-Applied Chemistry, Chalmers University of Technology, SE-41296 Gothenburg, Sweden
[g] Solid State Physics Division, Bhabha Atomic Research Centre, Mumbai, 400 085, India
[h] Soft Condensed Matter, Debye Institute for Nanomaterials Science, Utrecht University, Princetonplein 5, 3584 CC Utrecht, the Netherlands
‡ Equal contribution from the authors

Corresponding authors: Sugam@barc.gov.in; Krassimir.Velikov@unilever.com

Additional Details on the Computational Simulations.

The analysis of the last portion of the production trajectories was focused on the comparison of the configurations sampled in the different $ZnCl_2$ solutions with an average representative structure of the nanofiber in water with Na^+ ions. An estimation of the reorganization of the chains of the nanofiber, which was useful for a comparison with the experimental findings, was accomplished by checking the root mean deviations of their carbon atoms in relation to the reference structure. The positions of the metal ions in relation to the support and to the carboxyl head groups were examined in detail, together with hydrogen bonds, protonation states, and solvation effects. Visual inspection of the trajectories was also fundamental to disclose metal coordination, clustering, and adsorption locations in terms of chelation and trapping by the carboxyl moieties.

It is worth mentioning that due to the complex environments and to the large degree of freedom, it is very complicated to extend the number of models and the simulation time, to obtain a fully detailed molecular model or more realistic representations of the ions around these supramolecular arrangements. Experimental characterization at the atomic level is likewise difficult and only theoretical models can provide such descriptions deducing possible explanations of many of the effects observed experimentally. Although, the complex aggregation and full stabilization of TOCNF chains, water, ion and counter-ions are very slow processes to be disclosed with modelling (due to the extremely long simulation times - with the ion motion as the rate-determining step in the total convergence), the present simulations can provide explanations and ideas of the tendencies and trends of both the nanocellulose chains and the surrounding metal ions.

It may also be added here that there are other structures also, available in the literature, which are taken under consideration for modelling CNF such as hexagonal rosette structures. However, considering that our focus was on interfacial interactions, reactivity, ions adsorption, etc. and not on the determination of the most probable packing arrangements of the fibrils, we chose (to reduce the computational cost) this more simplified model that could give the general idea of interfiber interactions as well. This choice was based on our previous results (*Nanoscale*, 2019, 11, 22413–22422; *ACS Nano*, 2018, 12, 7028–7038) that demonstrated that we could use the designed scheme confidently to characterize the features mentioned above.

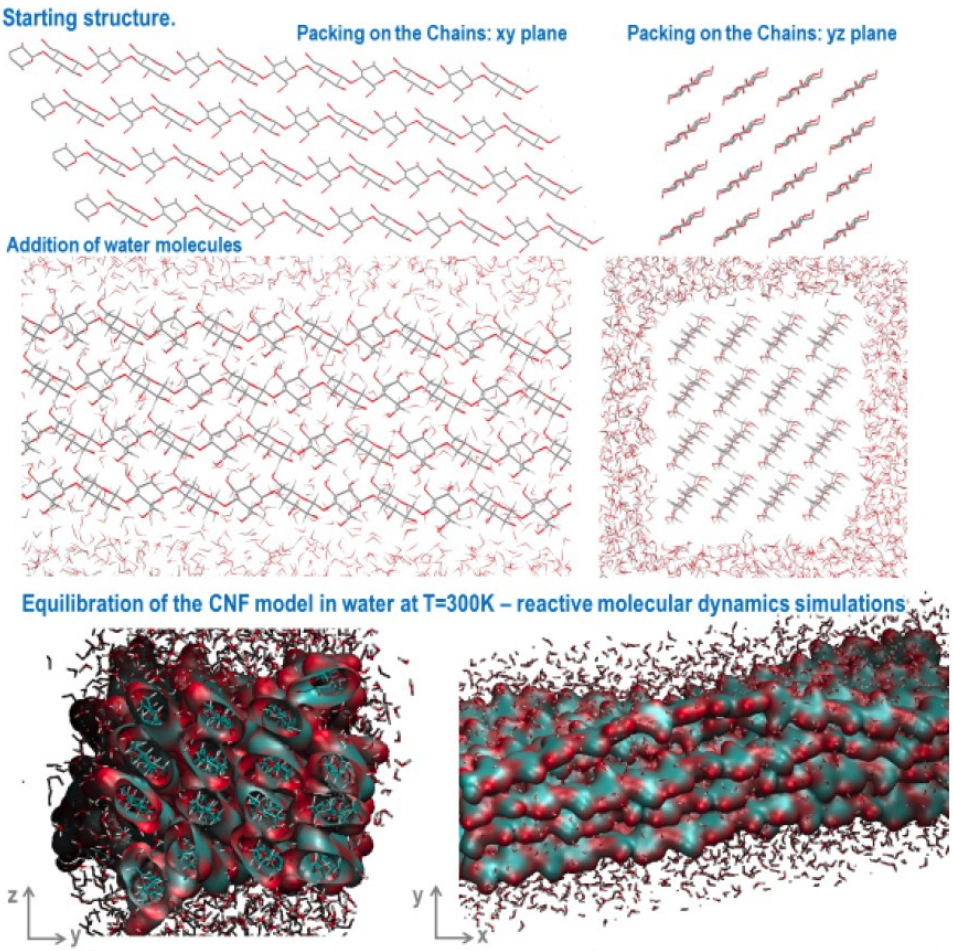

Figure S1. Cellulose nanofibrils model used in this study: The infinite length of the CNFs was rendered through a periodic supercell, with chains covalently bonded across the x border, whereas the CNF packing was controlled by adjusting the dimensions of the simulation box in the y and z directions. The crystal structure of the IB cellulose was determined by X-ray and neutron diffraction to create the 16 CNF chains made of 16 glucosyl residues each, which were aligned along the x-direction of the supercell. The behavior of the CNF model was tested through a series of short(hundreds of picoseconds) all-atom molecular dynamics (MD) simulations in the NPT ensemble, at 300 K and 1 atm. The volume of the system could change along the y and z directions that are perpendicular to the fibril axis (x-direction). The analysis of the MD trajectories confirmed the stability of the overall structure, which preserved its morphology and crystallinity.

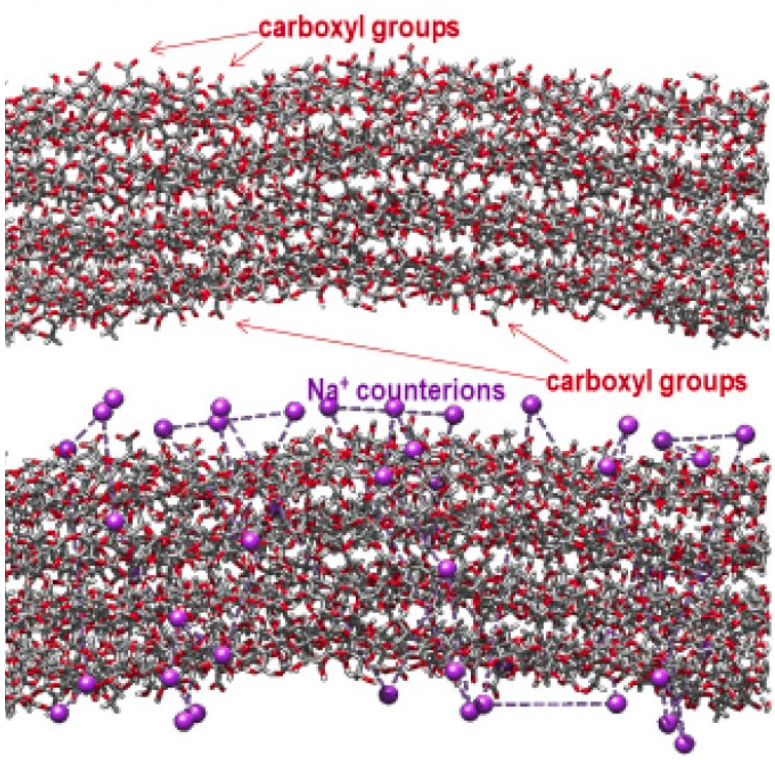

Figure S2. TOCNF model: The equilibrated configuration was subsequently modified to obtain a functionalized model with carboxyl groups. The procedure reflected the experimental TEMPO-mediated oxidation, where the exposed C6 primary hydroxyl groups of the surface (12 chains in our case) were selectively replaced with C6 carboxyl groups. Sodium counterions were positioned in close contact with the carboxyl groups.

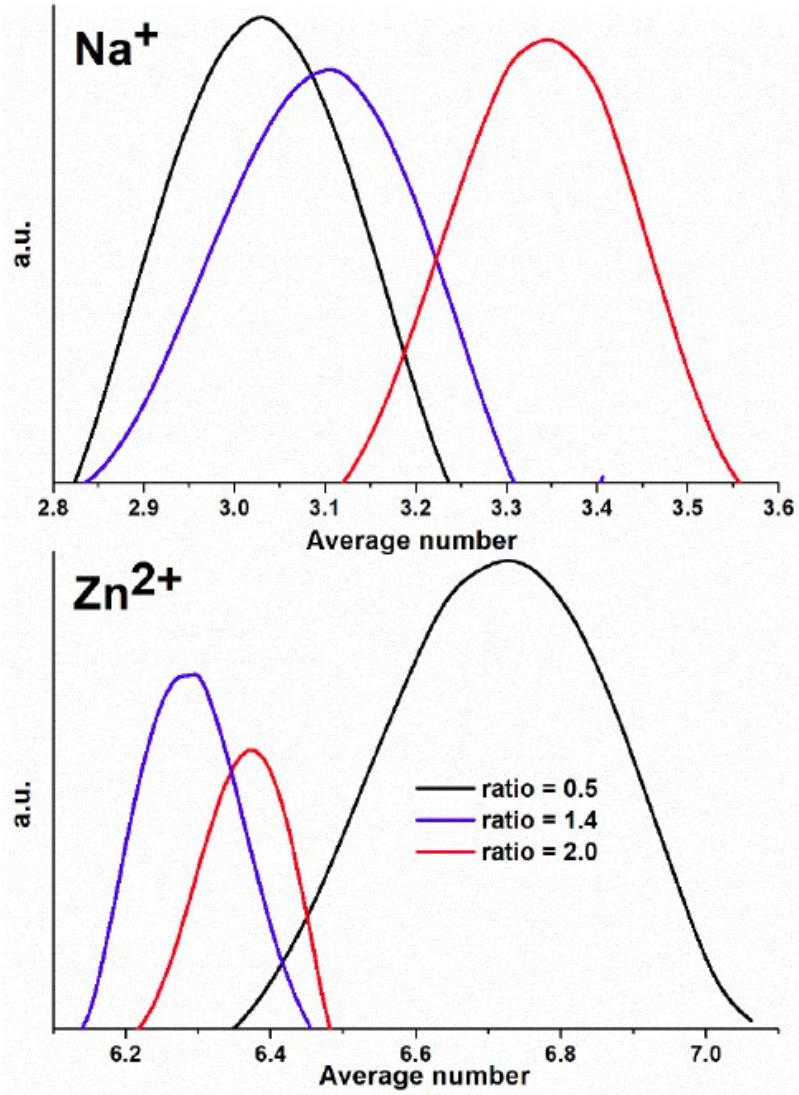

Figure S3. The average number of water molecules within 3 Å of each metal ion.

Table S1. Possible coordination of both Na^+ and Zn^{2+} ions to the carboxyl groups obtained considering an O-Na^+/Zn^{2+} distance of about 3.2 Å, whereas their permanence around the TOCNF fiber was identified choosing a maximum distance of approximately 5 Å from the TOCNF carbon atoms.

Salt concentration (mM)	Zn^{2+}/COO^- ratio	H (1.1 Å) O(COO-) %	Na^+ (3.2 Å) (O(COO-)) %	Zn^{2+} (3.2 Å) (O(COO-)) %	Na^+ (5 Å) C (TOCNF) %	Zn^{2+} (5 Å) C (TOCNF) %	Cl^- (5 Å) C (TOCNF) %
0.0	**0.0**	23	90	-	85	-	-
1.0	**0.5**	23	90	8	85	17	4
2.0	**1.4**	19	75	9	81	10	11
3.0	**2.0**	23	69	4	84	10	11

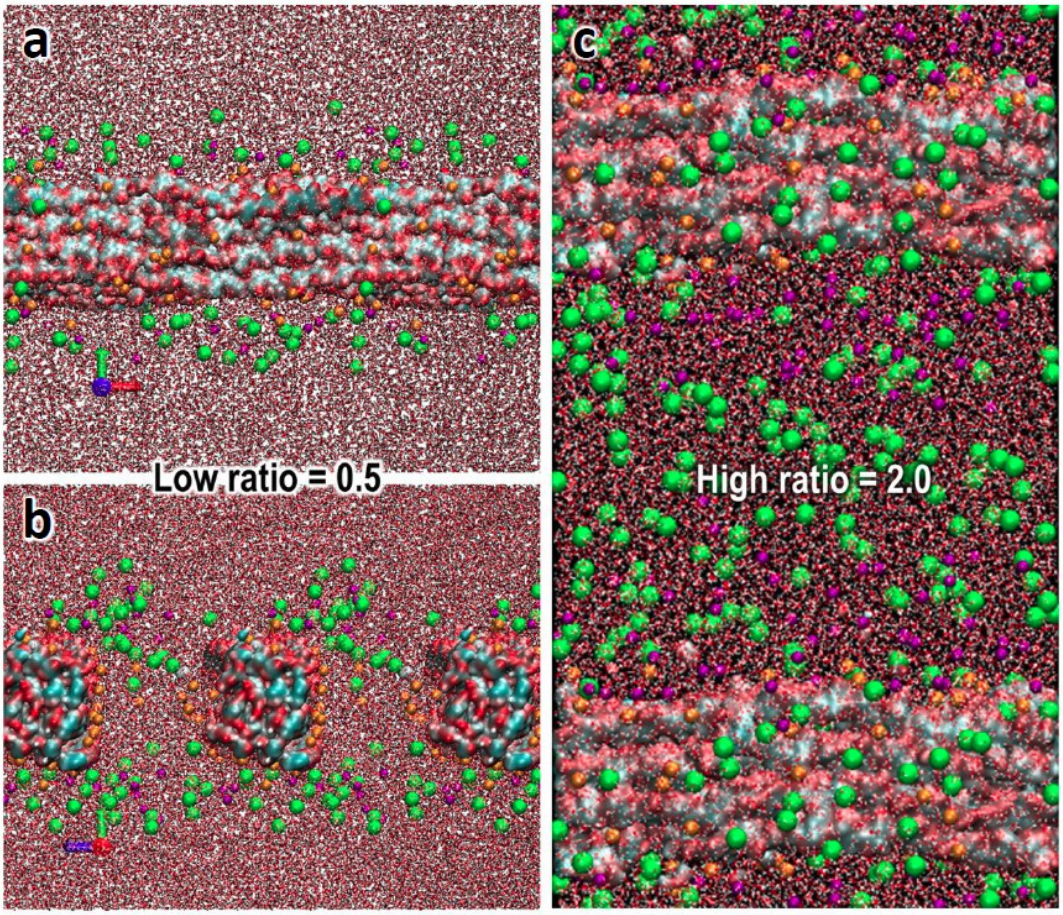

Figure S4. Snapshots extracted from the simulations at 0.5 and 2.0 Zn^{2+}/COO^- ratios. The fiber is rendered through a solvent accessible surface enveloping all the 16 chains colored according to the atom type: C=cyan, O=red, H=white. Zn^{2+}, Na^+, and Cl^- ions are magenta, orange and green spheres. Water molecules are displayed as lines. Periodic boundary conditions are visible in all the pictures to show the infinite length of the chains (a) and the separation between the various fibers in the different directions (b, c).

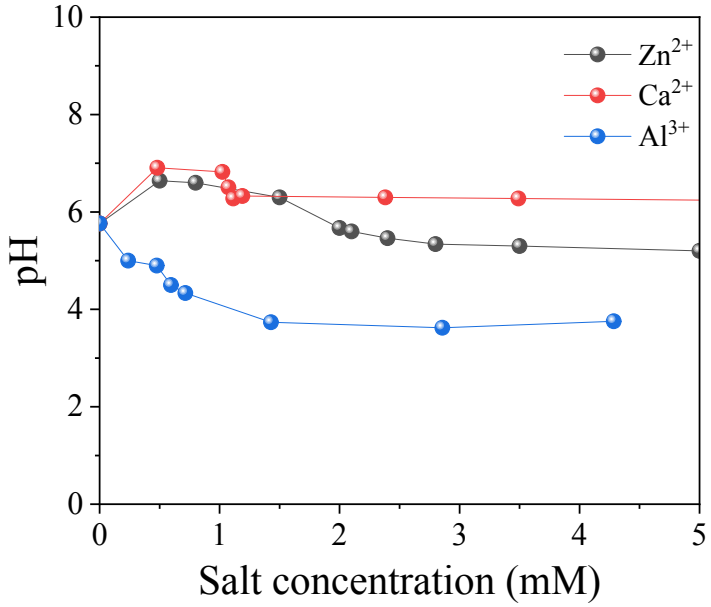

Figure S5. Variation in the pH of a TOCNF suspension (0.2 wt%) upon the incorporation of different concentrations of multivalent metal salts.

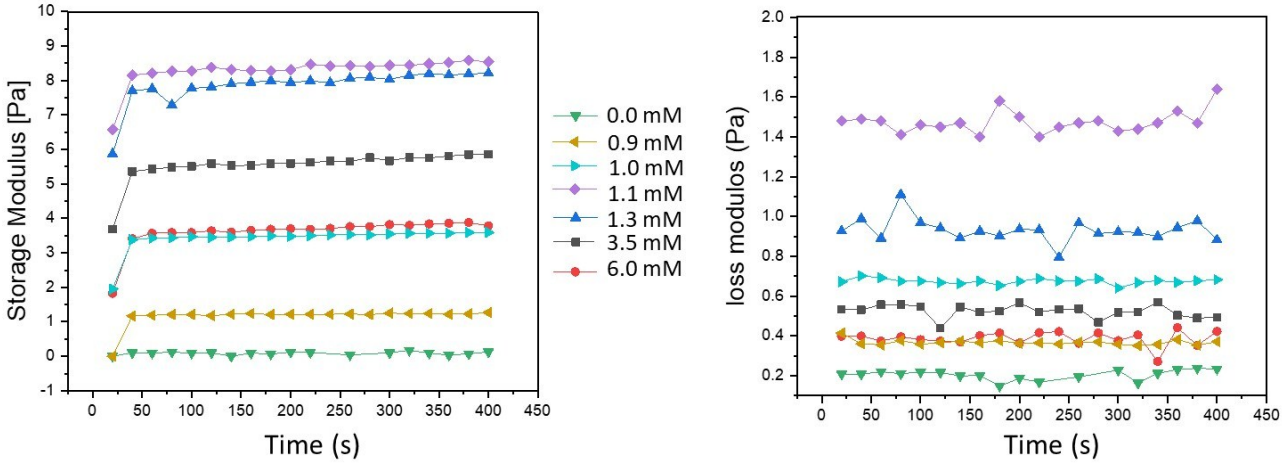

Figure S6. Rheological time sweep of TOCNF suspensions (0.1wt%) showing the storage (left) and loss (right) modulus at different zinc ion concentrations.

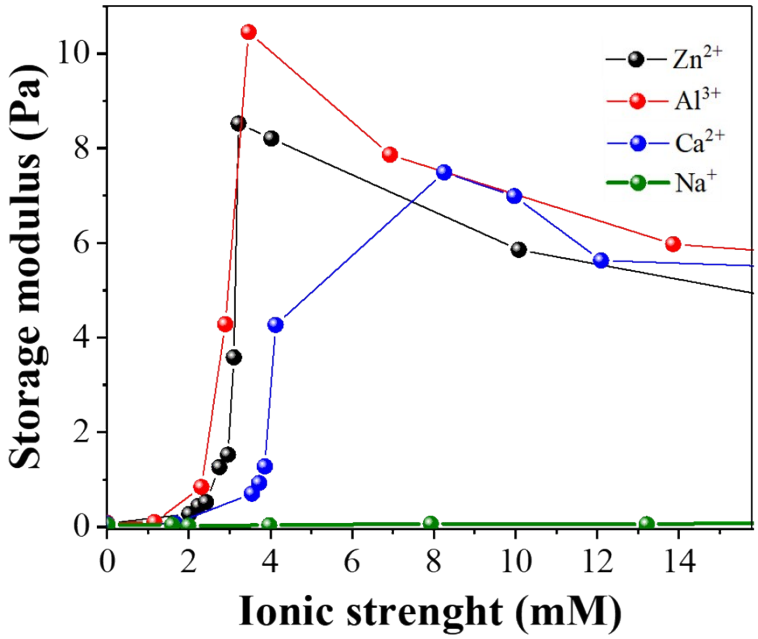

Figure S7. G´of TOCNF suspension (0.1 wt%) as a function of ionic strength with different metal salts at 1 Hz and 0.1% strain.

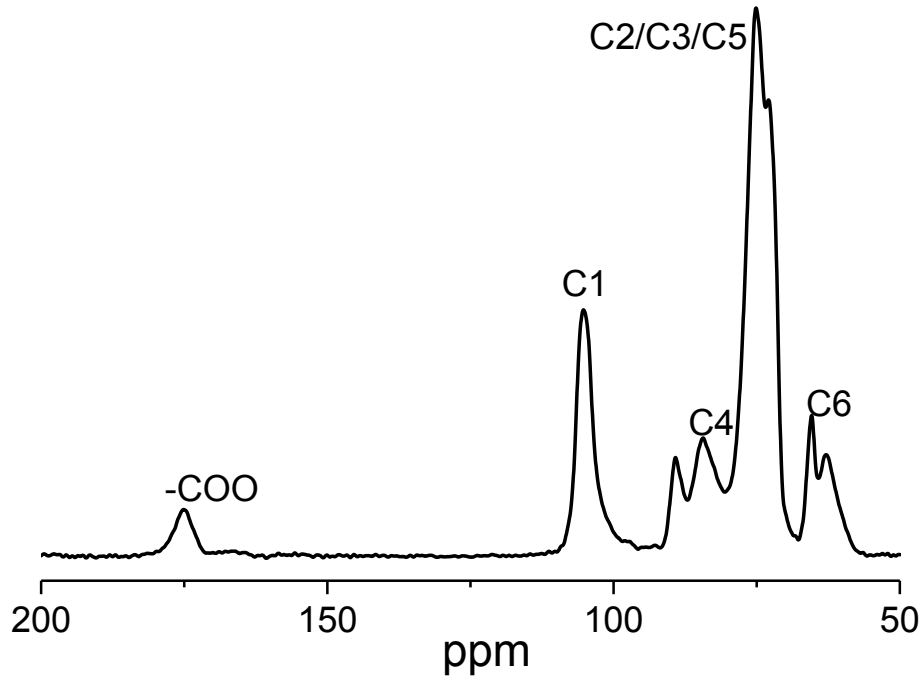

Figure S8. ^{13}C SS NMR of TOCNF used in this study. The amount of carboxyl groups was determined via ^{13}C SS NMR by dividing the ratio between the integral area of C1 peak [at 105 ppm] over the corresponding to the carboxyl groups [175 ppm] (resulting in 1 carboxyl group in every 4.5 glucose molecules).

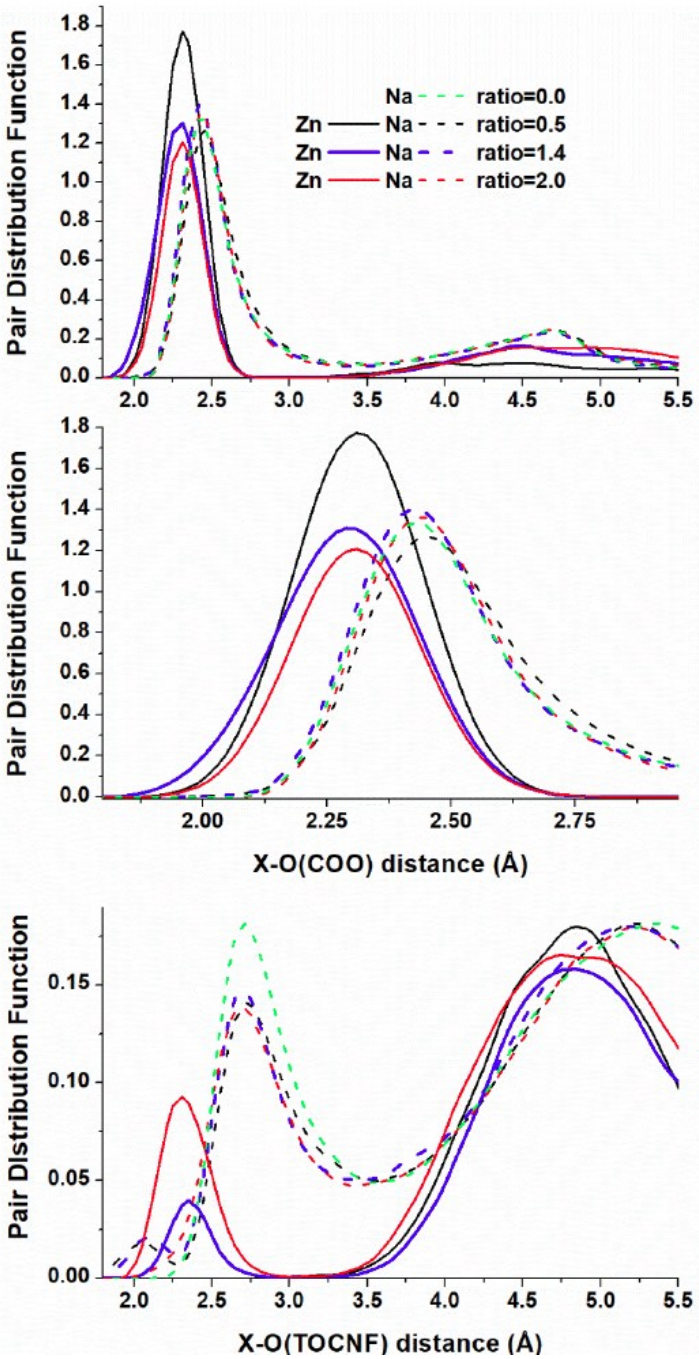

Figure S9. Atom-atom distribution functions. Top/middle (zoomed region): Zn^{2+}–carboxyl oxygens obtained from the last portions of the production trajectories (solid lines), Na^{+}–carboxyl oxygens (dashed lines). Bottom: Na^{+}/Zn^{2+}–all TOCNF oxygens (carboxyl oxygens excluded) obtained from the last portions of the production trajectories (dashed/solid lines).

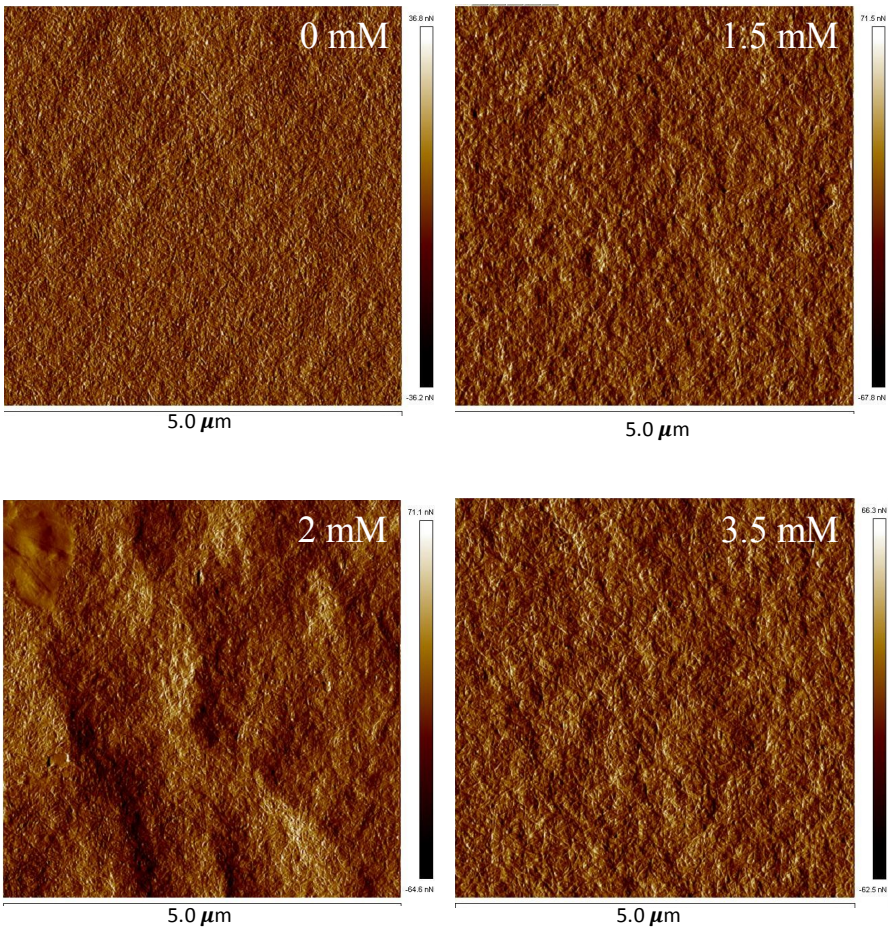

Figure S10. AFM micrographs of TOCNF films upon drying the hydrogels with variable salt concentration ($ZnCl_2$).

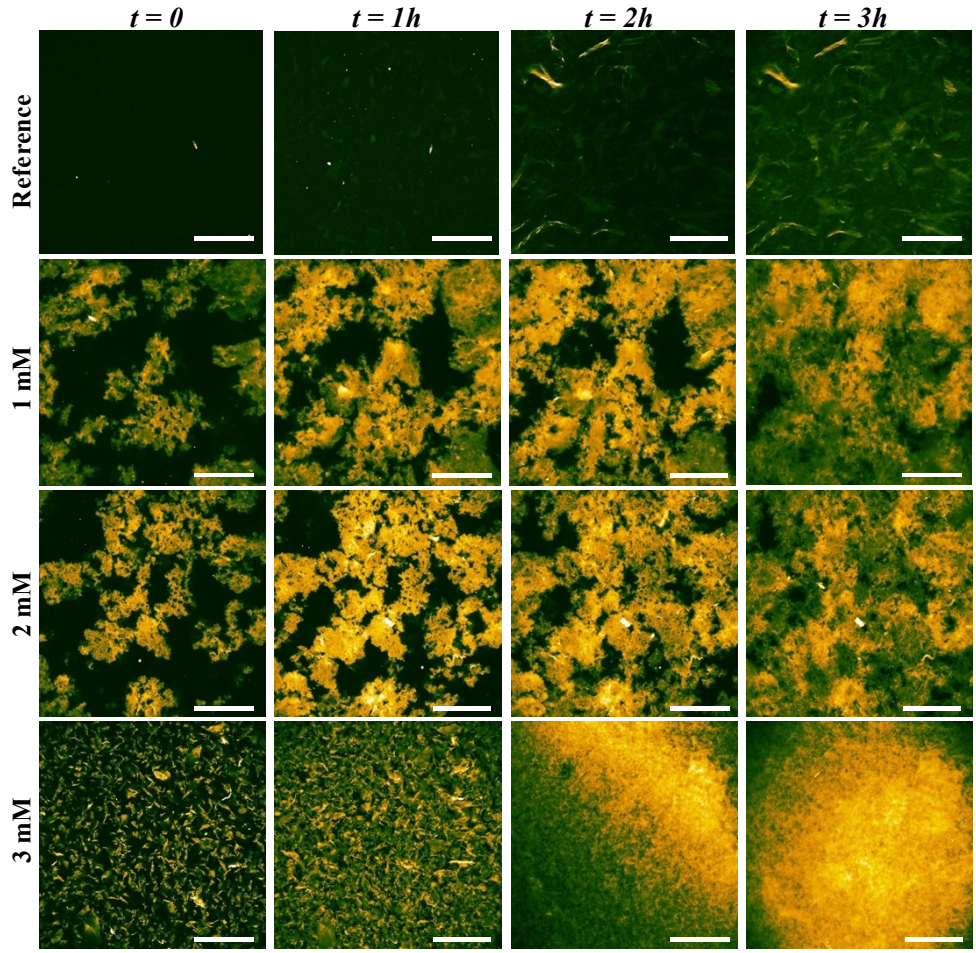

Figure S11. CLSM micrographs of TOCFN suspensions with varying metal salt concentration observed at different times: (**a**) Reference [0 mM]; (**b**) 1 mM; (**c**) 2 mM [C_0] and (**d**) 3 mM. Scale bar = 500 μm.

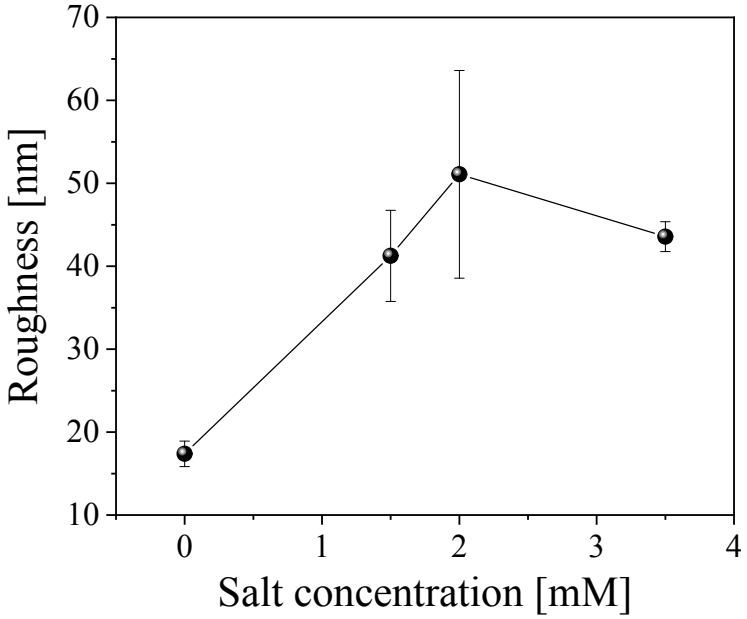

Figure S12. The roughness of TOCNF films with variable salt concentration measured by AFM.